ELSEVIER

Polymer 41 (2000) 2947–2960

polymer

Toughening and strengthening of polypropylene using the rigid–rigid polymer toughening concept
Part I. Morphology and mechanical property investigations

G.-X. Wei[a], H.-J. Sue[a,*], J. Chu[b], C. Huang[c], K. Gong[c]

[a]*Polymer Technology Center, Department of Mechanical Engineering, Texas A&M University, College Station, TX 77843-3123, USA*
[b]*Visteon Automotive System, Dearborn, MI 48121, USA*
[c]*Department of Polymer Material Science and Technology, South China University of Technology, Guangzhou, Guangdong 545007, People's Republic of China*

Received 18 February 1999; received in revised form 18 June 1999; accepted 22 June 1999

Abstract

The morphology and mechanical behavior of isotactic polypropylene (iPP) and Noryl blends were studied. It is found that the fracture toughness of iPP can be significantly improved by adding rigid Noryl without causing any reduction in modulus. Large Noryl particles (about 10–15 μm) are formed if no compatibilizers are utilized in the iPP/Noryl blend. The addition of a small amount of styrene–ethylene–propylene (SEP) compatibilizer causes a significant reduction in Noryl particle size. A noticeable improvement in particle–matrix interfacial adhesion is also observed. Also, the energies required for both crack initiation and crack propagation of iPP are greatly increased. The results show that phase morphology has a great effect on the mechanical performance of these blends. The structure–property relationship in iPP/Noryl blends is discussed in detail.

Keywords: Isotactic polypropylene; Noryl; Rigid–rigid polymer toughening

1. Introduction

Isotactic polypropylene (iPP) is known to exhibit low impact strength at temperatures close to or below room temperature, which greatly limits its engineering structural applications. In recent years, many studies have been conducted to improve the impact strength of iPP. Rubber modification has been shown to be effective in toughening iPP even at low temperatures (i.e. −20°C) [1,2]. Unfortunately, the accompanying penalty from rubber toughening usually manifests as a noticeable reduction in modulus and scratch/mar resistance. Consequently, significant research is needed to overcome the above drawbacks in order for polymer products to compete successfully in automotive applications.

The reduction in scratch resistance has been attributed to the addition of rubber which decreases the modulus of thermoplastic olefin (TPO). However, the scratch resistance of TPO is not improved with further addition of inorganic fillers, which is supposed to increase the modulus of TPO [3]. Although a fundamental knowledge concerning scratch resistance in polymers is still lacking, it is believed that modulus, yield/brittle stress, yield/brittle strain, dynamic friction coefficient and toughness could significantly influence scratch resistance in polymers. A delicate balance among these variables has to be reached in order to achieve a TPO system with both improved toughness and acceptable scratch resistance.

The recently introduced rigid–rigid polymer toughening concept [4–8] has provided new routes for structural uses of polymeric materials. Based on this new concept, it is possible to improve both modulus and toughness of iPP by incorporating a rigid engineering polymer, such as polycarbonate, polyethylene terephthalate, and polyphenylene oxide (PPO). Since Noryl (a mixture of PPO and high impact polystyrene (HIPS)) has been shown to be effective in toughening semi-crystalline nylon 6,6 [6,7], it is chosen to toughen iPP for the present study. It is anticipated that the Noryl particles can serve as stress concentrators to trigger cavitational mechanisms, such as crazing and interfacial debonding, and to relieve the crack tip triaxial stress constraint, which then leads to massive shear banding in the iPP matrix.

* Corresponding author. Tel.: +1-409-845-5024; fax: +1-409-862-3989.
E-mail address: hjsu@acs.tamu.edu (H.-J. Sue).

0032-3861/00/$ - see front matter
PII: S0032-3861(99)00454-1

As we know, iPP and Noryl are immiscible in each other due to significant differences in their polarity and solubility parameters. For a blend consisting of two immiscible polymers, there are two important factors that affect the mechanical properties of the blend [9,10]: the morphology of the dispersed phase and the interfacial adhesion between the dispersed phase and the matrix. In order to improve both particle dispersion and interfacial adhesion, compatibilizers can be added to the blends to mediate an attractive interaction between the immiscible polymer components. The addition of a second phase material to a semi-crystalline polymer matrix may also affect crystallinity, spherulite size, and lamella thickness. This may have significant effects on the physical and mechanical properties of the polymer blends [11–14]. In the present study, the styrene–ethylene–propylene (SEP) diblock copolymer is chosen to compatibilize iPP/Noryl blend. It is expected that the styrene block will be miscible with the Noryl phase and the ethylene–propylene block will be compatible with the iPP matrix.

This paper, which is part of a larger effort to improve both scratch resistance and impact resistance in TPOs, focuses on utilizing rigid Noryl to improve both modulus and toughness of iPP. The effects of Noryl and SEP compatibilizer on crystallinity and spherulite size of iPP are studied. The relationships between phase morphology and mechanical properties of these polymer blends are discussed in detail.

2. Experimental

2.1. Materials

The iPP used to conduct this research has $M_n = 100\,000$ and $M_w = 368\,000$, with a melt flow rate index (MFI) of 2.5. The Noryl pellets, Noryl™ PX0844, a mixture of PPO and HIPS, which has a glass transition temperature (T_g) of 150°C, were received from the General Electric Company. The styrene–ethylene–propylene (SEP) diblock copolymer with T_g of −58°C for the EP block and 95°C for styrene block (Kraton-G1701), which was used as a compatibilizer, was obtained from Shell Chemical. All polymers used in this research are commercial products. Blends of iPP/10% Noryl, iPP/10%Noryl/2%SEP and iPP/10%Noryl/5%SEP were prepared using a research grade roll milling machine at a roll temperature of 200°C.

2.2. Specimen preparation

The iPP, iPP/10%Noryl, iPP/10%Noryl/2%SEP and iPP/10%Noryl/5%SEP blends were compression molded into thin sheets (4 mm thick) at 200°C. Cooling water was used to quickly cool the plaques. Single-edge-notch three-point bend (SEN-3PB) specimens were cut from the compression molded plaques. Samples were machined to reach the final dimensions of $63.5 \times 12.7 \times 4\ mm^3$. The SEN-3PB bars were notched with a 250 μm radius notch cutter to a notch depth of 5.5 mm, followed by liquid nitrogen-chilled razor blade tapping to open a sharp crack to a total depth of about 6.4 mm ($a/W = 0.5$–0.55) for *J*-integral fracture toughness measurements. Tensile specimens were cut from the compression molded plaques and machined to required dimensions designated by ASTM method (D 638M-96).

2.3. DSC measurements

Differential scanning calorimetry (DSC) measurements were performed using Perkin–Elmer DSC (model Pyris 1). All scans were conducted in a nitrogen environment at a heating/cooling rate of 10°C/min. Melting temperature (T_m) was determined from the heating curve while the crystallization temperature (T_c) was determined from cooling. The heat of fusion for 100% crystallinity of iPP was taken as 209 J/g for crystallinity calculations [15].

2.4. Dynamic mechanical analysis

The dynamic mechanical behavior of the neat- and toughened-iPP was studied using dynamic mechanical spectroscopy (DMS) machine, Rheometrics RMS-800, in a torsional mode, with 2.5°C per step. A constant strain amplitude of 0.01% and a fixed frequency of 1 Hz were employed. The samples were tested at temperatures ranging from −140 to 160°C. The T_g was assigned to be the tan δ peak temperature.

2.5. Microscopy

The morphology in neat-iPP and iPP blends was investigated using transmission optical microscopy (TOM), scanning electron microscopy (SEM), and transmitted electron microscopy (TEM). In the TOM investigation, thin sections with thickness of about 20 μm were obtained by polishing, following the procedure described by Holik et al. [16]. The thin sections were then examined using an Olympus BX60 optical microscope under both bright field and cross-polarization conditions to analyze the Noryl particle size and iPP spherulites.

SEM investigations were performed on polished specimens to study the Noryl particle size and iPP matrix spherulite feature in all blends. In this experiment, specimens were polished following the same procedure as that in the TOM investigation to obtain flat and smooth surfaces. These polished specimens were subsequently immersed in a solution containing 1.3 wt% potassium permanganate, 32.9 wt% dry H_3PO_4 and 65.8 wt% concentrated H_2SO_4 for 24 h [17,18]. SEM studies were also performed to analyze fracture surface features of the *J*-integral tested specimens. All specimens were coated with a 300 Å layer of Au–Pd and studied using the JSM-6400 SEM operated at an accelerating voltage of 15 kV.

For the TEM experiments, specimens were carefully trimmed to an appropriate size (i.e. $5 \times 5\ mm^2$) and

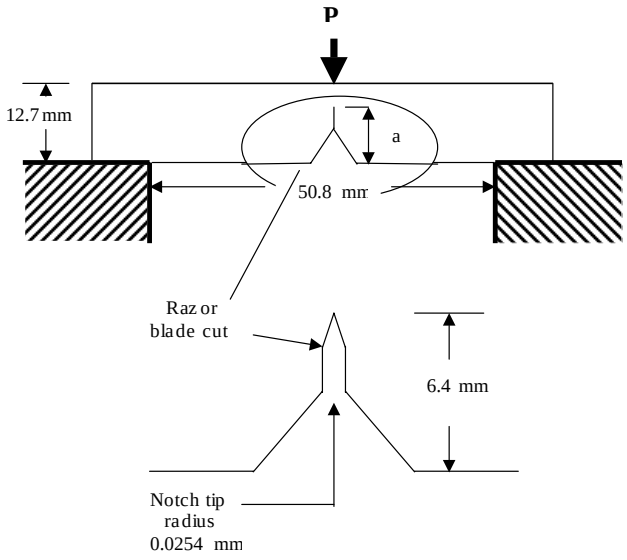

Fig. 1. Schematic of the three-point bend test specimen used for the *J*-integral test.

embedded in DER 331 epoxy/diethylenetriamine (12:1 ratio by weight). The epoxy was cured at room temperature overnight. The cured block was then further trimmed to a size of about 0.3×0.3 mm^2. A diamond knife was used to face off the trimmed block prior to RuO_4 staining. The faced-off block was exposed to the vapor of an aqueous RuO_4 solution (0.5% by weight) for 2.5 h. Ultra-thin sections, ranging from 60 to 80 nm, were obtained using a Reichert–Jung Ultracut E microtome with a diamond knife at room temperature. The thin sections were placed on 200-mesh formvar-coated copper grids and examined using a JEOL 2000FX ATEM operated at an accelerating voltage of 100 kV.

2.6. Mechanical testing

The *J*-integral test was done according to ASTM E813-89 using a multiple-specimen technique at room temperature. The schematic of the three-point bend test specimen is shown in Fig. 1. An Instron (Model 4411) screw-driven mechanical testing machine was used to perform the measurements at a crosshead speed of 2 mm/min. During testing, a series of specimens were loaded and unloaded to different predetermined deflections, i.e. different levels of crack growth. The load–deflection curve was recorded and monitored using a computer data acquisition program which allowed the potential energy (area under the load–deflection diagram) to be calculated. After unloading, each specimen was immersed in liquid nitrogen for 3 min and broken immediately to cause brittle fracture. The extent of crack growth was measured from the fracture surface using an optical microscope. The *J*-integral value was calculated using the following expression:

$$J = \frac{2U}{B(W - a)}$$

where U is the input energy to the specimen given by the area under the load–displacement curve, B the thickness of the specimen, W the width of the specimen and a the crack length.

The calculated *J*-values were then plotted against the advanced crack length, Δa, to obtain a *J–R* curve. Using this method, the J_c-values were determined at the point of intersection between the *J–R* curve and the blunting line ($J = 2\sigma_y \Delta a$, where σ_y is the yield stress).

Tensile tests were carried out following ASTM D 638M-96 using Type M-II specimen geometry. The tests were performed at a crosshead speed of 2 mm/min and at room temperature.

3. Results and discussion

3.1. Thermal analysis

It is well known that the crystallinity of semi-crystalline polymers plays a significant role in determining their mechanical properties and fracture behavior. The addition of second phase particles such as rubber and inorganic fillers may affect crystallinity and spherulite morphology of iPP. Greco et al. [11,19], reported that polyisobutylene (PIB) and ethylene–propylene rubber (EPR) acted as nucleation agents to reduce crystallinity and spherulite size of PP. On the other hand, Chou et al. [20], found that the crystallinity of PP was independent of the EPR rubber content while the spherulite size was dramatically decreased by the addition of EPR. Pukanszky et al. [21] and Rybinkar [22] reported

Table 1
Crystallinity (X_c), melting temperature (T_m), crystallization temperature (T_c) and T_g of iPP and toughened-iPP

Materials	X_c[a] (%)	T_m at peak (°C)	T_c at peak (°C)	T_g[b] (°C)		
				iPP	SEP	Noryl
iPP	39.7	167	114	5	–	–
iPP/10%Noryl	40.7	166	117	6	–	150
iPP/10%Noryl/2%SEP	41.0	167	117	5	− 52	151
iPP/10%Noryl/5%SEP	41.0	167	117	4	− 53	152

[a] Crystallinity normalized by sample weight.
[b] Temperature at which tan δ curve of DMS at 1 Hz is a maximum.

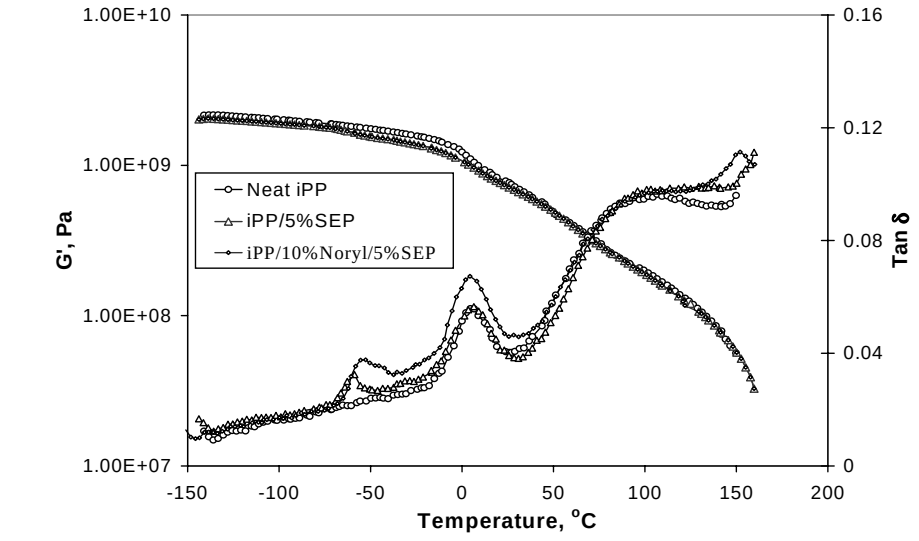

(a)

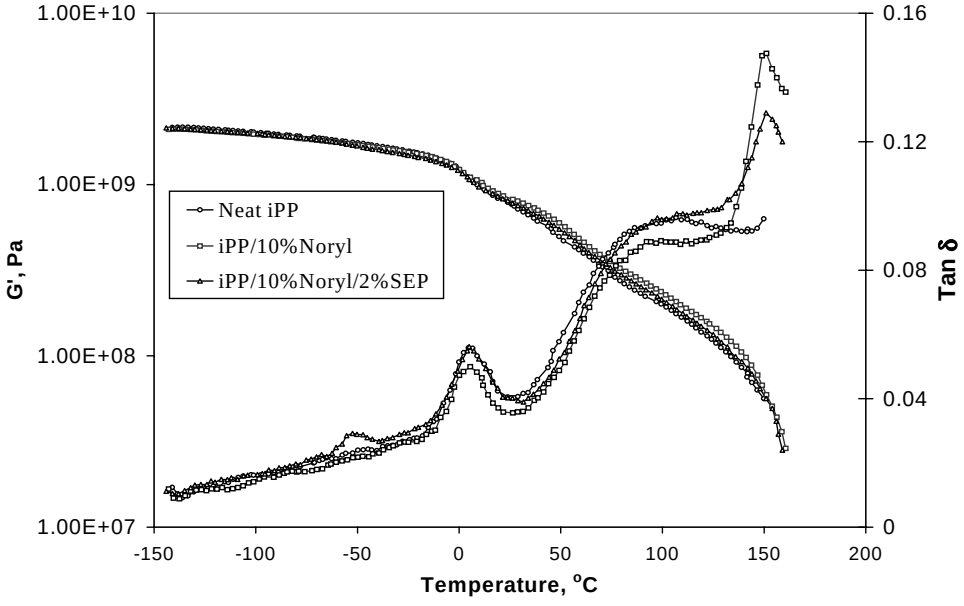

(b)

Fig. 2. Dynamic mechanical spectra of iPP vs. toughened-iPP. DMS of: (a) iPP, iPP/5%SEP and iPP/10%Noryl/5%SEP; (b) iPP, iPP/10%Noryl and iPP/10%Noryl/2%SEP.

that mineral fillers may strongly affect the crystallization process of semi-crystalline polymers in a quantitative and qualitative manner. Rybnikar observed that the number of nucleation centers was greater for filled PP than for unfilled PP. This led to the growth of a large number of smaller spherulites. The effect of the second phase materials on crystallinity and spherulite morphology depends on blend composition and structure of the second phase. To evaluate extent to which Noryl and SEP influence the crystallization process in iPP blends, DSC analyses were performed on neat-iPP and its blends. The results are summarized in Table 1. It is noted that both crystallinity and melting temperature (T_m) is about the same for all samples. The addition of Noryl and SEP does not have a significant effect on the crystallinity and the melting behavior of iPP. Since the melting behavior observed in DSC is determined primarily by the characteristics of crystallites, this feature suggests that the crystalline structure in iPP at the size scale of lamellae is not strongly affected by the presence of Noryl and SEP. In fact, our small angle X-ray (SAXS) analysis results confirm that lamella thickness and the long period of crystalline phase in all specimens are the same, i.e. 5 and 15 nm, respectively [23]. On the other hand, the crystallization temperature is about 3°C higher for iPP/Noryl and iPP/Noryl/SEP blends than that of neat-iPP. This is an indication that Noryl acts as a nucleation agent which may affect the

Table 2
Selected mechanical properties of iPP and toughened-iPP

Materials	Young's modulus E (GPa)	Yield stress (MPa)	J_c (kJ/m^2)	Storage shear modulus 25°C	G' (MPa) 80°C
iPP	1.61 ± 0.06	35.5 ± 0.5	3.0	787	270
iPP/10%Noryl	1.79 ± 0.08	30.5 ± 0.7	14.5	830	325
iPP/10%Noryl/2%SEP	1.55 ± 0.04	28.7 ± 1.2	28.1	805	298
iPP/10%Noryl/5%SEP	1.41 ± 0.05	30.0 ± 0.6	19.2	726	271

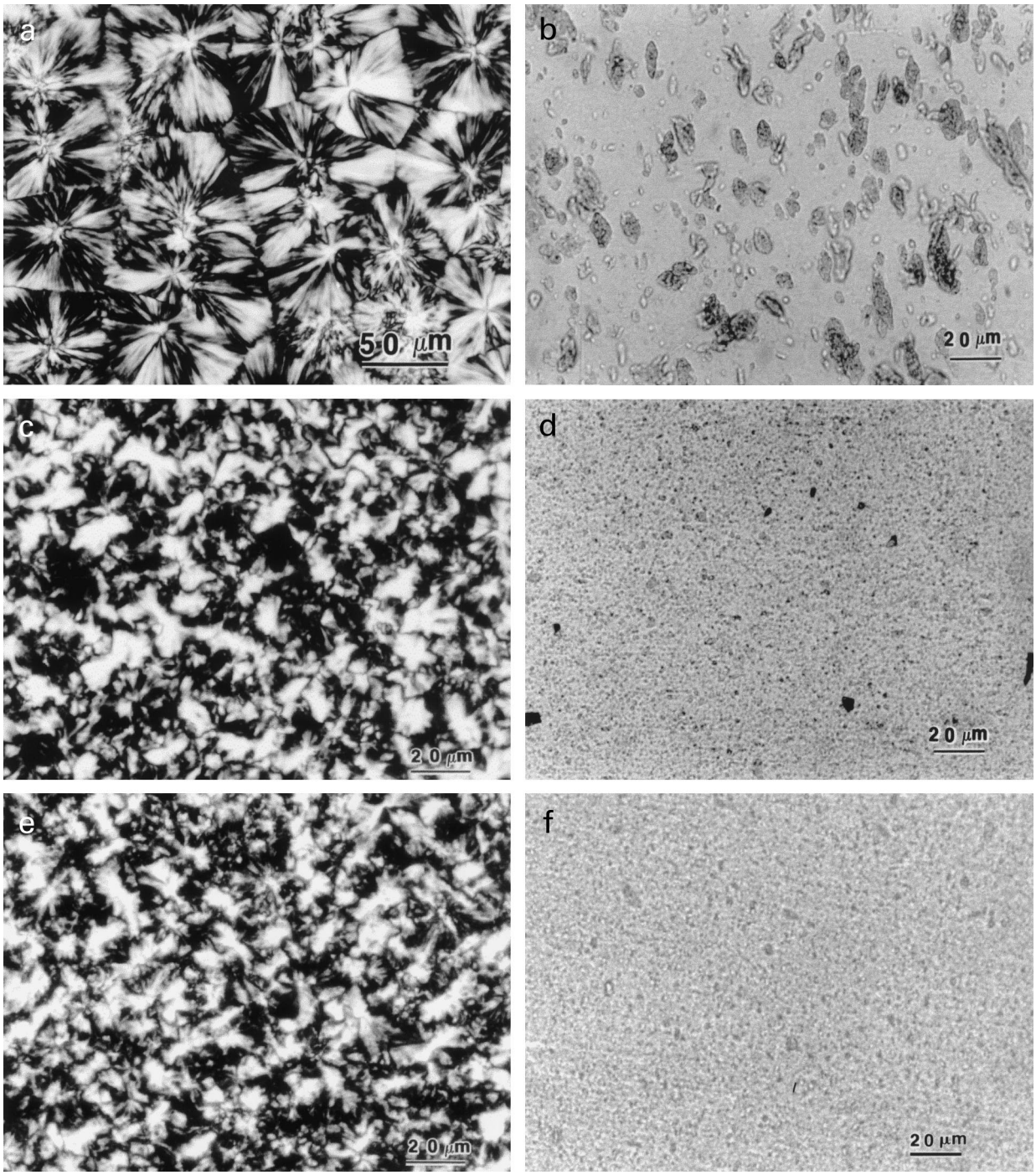

Fig. 3. Transmission optical micrographs of: (a) iPP; (b,c) iPP/10%Noryl; (d,e) iPP/10%Noryl/2%SEP; and (f,g) iPP/10%Noryl/5%SEP taken under (a,c,e,g) cross-polarized and (b,d,f) bright field.

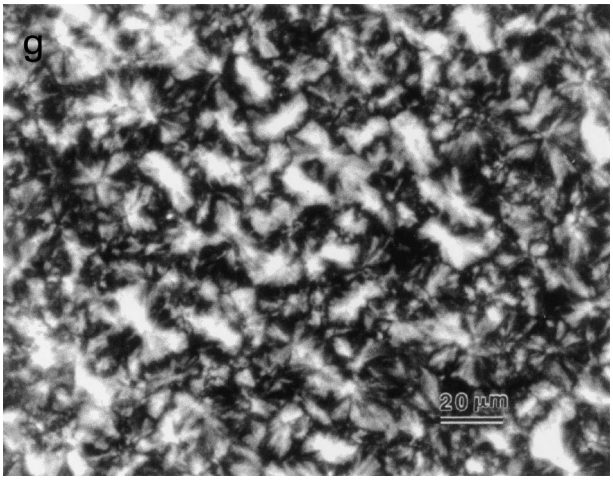

Fig. 3. (*continued*)

morphology of iPP spherulites. This feature will be further discussed when TOM and SEM results are presented.

3.2. Dynamic mechanical analysis

The dynamic mechanical spectra of iPP and toughened-iPP are shown in Fig. 2. For comparison purposes, the DMS spectrum of the 5% SEP-modified iPP is also plotted. The T_gs of all the blends are listed in Table 1. As shown, the presence of well-separated tan δ peaks of iPP, SEP and Noryl indicates a clear phase separation among them. The maximum tan δ of iPP does not shift with the addition of Noryl or SEP. However, the tan δ peaks of SEP shift to a higher temperature (about 5°C increase) with the addition of Noryl. This suggests that SEP and Noryl are partially compatible (i.e. styrene block in SEP is compatible with Noryl). The addition of SEP into iPP/Noryl blend can significantly reduce Noryl particle size. The T_g of Noryl is discernible even though it is close to the melting point of iPP. It is interesting to note that the T_g of Noryl is not affected by the SEP while the tan δ peak intensity is

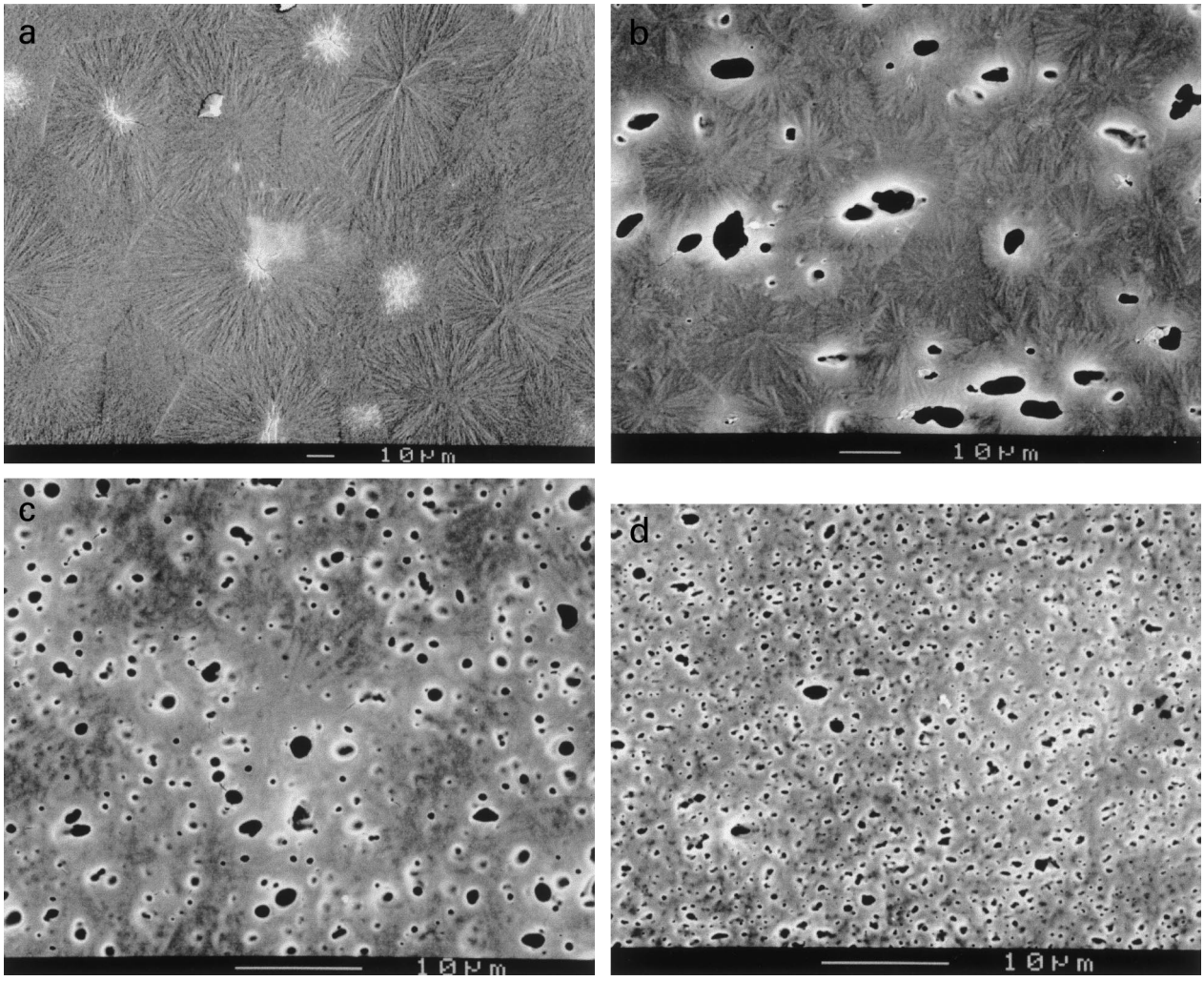

Fig. 4. Scanning electron micrographs of etched surfaces of: (a) iPP; (b) iPP/10%Noryl; (c) iPP/10%Noryl/2%SEP; and (d) iPP/10%Noryl/5%SEP. Spherulites cannot be observed on SEP-compatibilized iPP/Noryl blends (see (c) and (d)).

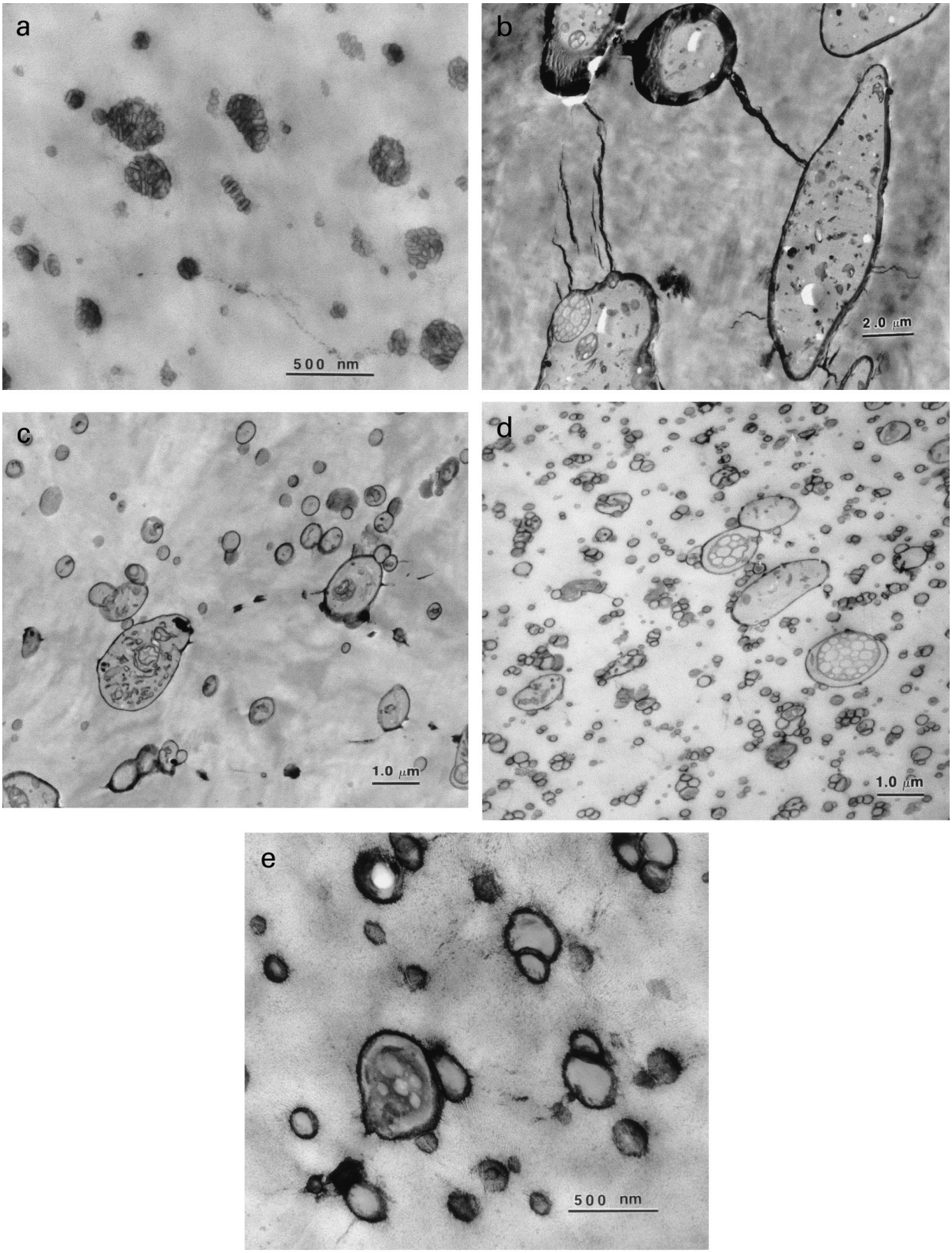

Fig. 5. Transmission electron micrographs of: (a) iPP/5%SEP; (b) iPP/10%Noryl; (c) iPP/10%Noryl/2%SEP; (d) iPP/10%Noryl/5%SEP at low magnification; and (e) iPP/10%Noryl/5%SEP at high magnification.

decreased with increasing SEP content. This phenomenon further confirms that SEP strongly interacts with Noryl. The reason the T_g of Noryl does not seem to shift is because of the low content of styrene block in SEP and the low amount of SEP utilized. The T_g of styrene block in SEP is not detected because the tan δ peak of styrene block overlaps with the hump of iPP at temperature around 100°C.

The shear storage moduli of all specimens are reported in Table 2. The addition of 10% Noryl particles increases the shear storage modulus of iPP, especially at higher temperatures (>80°C). This indicates that the heat deflection temperature of iPP is likely to be increased. However, this property is slightly decreased by the addition of SEP. Upon further addition of SEP, a larger drop of shear moduli is observed (Table 2). The change of the shear moduli is primarily due to the addition of the second phase particles. The addition of rigid Noryl increases the shear modulus of iPP while the addition of soft SEP decreases the shear modulus of iPP/Noryl blend.

3.3. Morphology observations

Transmission optical micrographs of polished thin sections (about 20 μm) of neat- and toughened-iPP samples are shown in Fig. 3. The neat-iPP forms well-defined spherulites during cooling (Fig. 3(a)). The average size of these spherulites is about 60 μm. When iPP was blended with 10% Noryl, large and non-uniform Noryl particles (about 10–15 μm in diameter) (Fig. 3(b)) are formed while the spherulite size is reduced approximately to 20 μm (Fig. 3(c)). As expected, the incorporation of 2% SEP compatibilizer into the iPP/10%Noryl blend makes Noryl particles much smaller and more uniform than that of the iPP/Noryl blend (Fig. 3(d)). Again, the spherulite size of iPP is reduced to about 20 μm (Fig. 3(e)). The boundaries between the spherulites are not distinct and the shape of the spherulites is more ribbon-like. When the SEP is increased to 5%, the Noryl particle size and iPP spherulites are optically similar to those of 2% SEP-modified iPP/10%Noryl blend (Fig. 3(f) and (g)). Noryl particles in SEP-compatibilized iPP/Noryl are too small to be discernable using TOM (Fig. 3(d) and (f)). From the optical microscopy study, it is evident that the addition of SEP has a significant effect on the Noryl particle size, the dispersion of Noryl particles and on the crystalline morphology in iPP. Unfortunately, detailed information about particle size and crystallite morphology cannot be observed unambiguously using TOM due to its low resolution. SEM is therefore employed.

When iPP and its blends are etched with an etching solution and investigated using SEM, the differences in spherulite features as well as the Noryl particle size in iPP blends are clearly revealed (Fig. 4). Well-developed spherulites with clear boundaries between spherulites in neat-iPP can be unambiguously observed (Fig. 4(a)). This is consistent with TOM result (Fig. 3(a)). Small but well-formed spherulites in iPP/Noryl specimen are clearly shown (Fig. 4(b)). No distinct spherulites can be detected in the SEP-compatibilized iPP/Noryl blends (Fig. 4(c) and (d)). The iPP/Noryl blend with a higher SEP content results in even smaller Noryl particles (compare Fig. 4(c) and (d)). Both TOM and SEM are unable to reveal the SEP phase. To determine the exact Noryl particle morphology and the reason for SEP to be so effective in reducing Noryl particle size, TEM investigations are conducted on iPP/5%SEP, iPP/10%Noryl, iPP/10%Noryl/2%SEP, and iPP/10%Noryl/5%SEP blends.

The TEM micrographs of the iPP blends are given in Fig. 5. It is clearly shown that the SEP is a two-phase diblock copolymer (Fig. 5(a)) which is consistent with the information provided by Shell Chemical [24]. The phase separation between iPP and SEP is well maintained during blending. This phenomenon is consistent with the test results of DMS, which indicates a clear phase separation between them. Blending iPP with Noryl alone results in large irregular elliptical Noryl particles in the iPP matrix (Fig. 5(b)). The rubber phase (which appears dark due to RuO_4 staining) and sub-inclusions inside the Noryl particles, which are characteristics of HIPS, are observed. The thick, dark layer located at the interface of iPP and Noryl is believed to be the rubbery phase from HIPS. When 2% by weight of SEP is added to the iPP/10%Noryl blend, small elliptical Noryl particles are formed (Fig. 5(c)). The average size of these particles, which is about 0.8 μm, is much smaller than that of iPP/10%Noryl (comparing Figs. 3(b) and 5(b)). A careful inspection reveals that a thin, dark layer of SEP surrounding Noryl particles is formed. No individual SEP phase is observed. This indicates that SEP prefers to reside at the interface between iPP and Noryl particles. The TEM micrograph of iPP/10%Noryl/5%SEP blend further confirms this observation. After 5% by weight of SEP is added into iPP/10%Noryl blend, much smaller Noryl particles (0.2–0.5 μm) are produced (Fig. 5(d)). A thicker SEP layer surrounding Noryl particles is present as shown in Fig. 5(e). It is interesting to note that crystalline texture of iPP seem to penetrate into the SEP phase, suggesting a good compatibility between these two phases. It is also observed that the thick SEP-sheathed Noryl particles tend to promote aggregates (Fig. 5(d)), which may have a negative effect on toughness. Again, no individual SEP phase is observed even though the SEP content is as high as 5% by weight.

It is noticed that increasing the SEP content from 2 to 5% by weight only reduces the Noryl particle size to a small extent (from about 0.8 to 0.2–0.5 μm). However, this increase causes the formation of a thick SEP layer between the iPP and Noryl particles. Aggregation of Noryl particles, which may deteriorate the effectiveness of toughening, may be caused by the presence of the thick SEP layer. It is possible that the addition of an even smaller amount of SEP, say, 0.5%, may be effective in dispersing Noryl particles and maintaining a good interfacial adhesion.

3.4. Tensile properties

The moduli and yield stress of iPP and its blends are

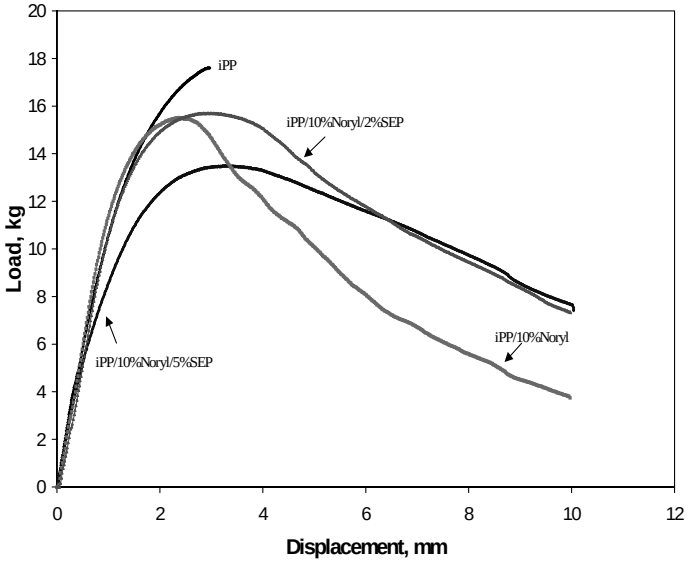

Fig. 6. Typical load–displacement curves of iPP vs. toughened-iPP.

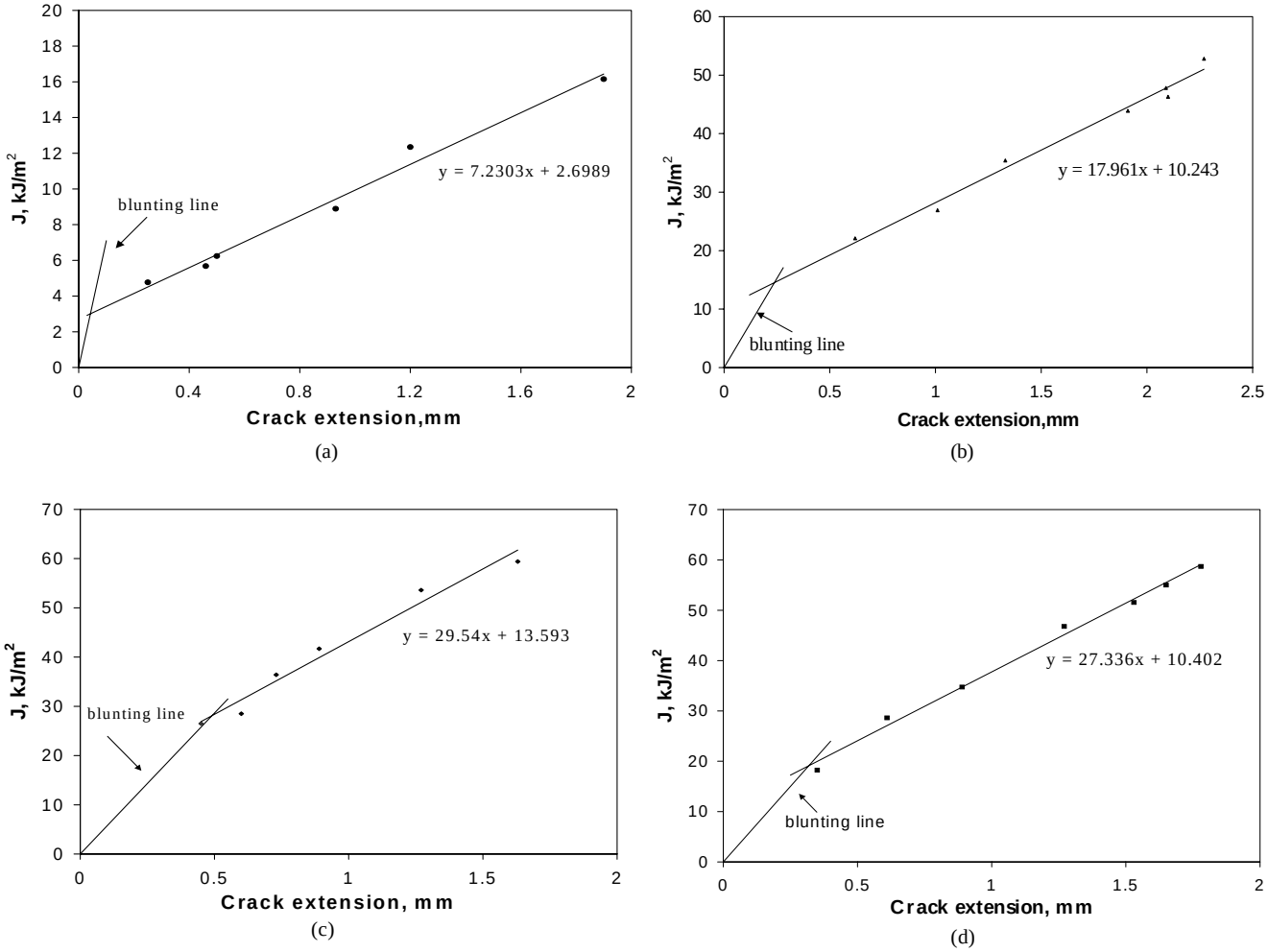

Fig. 7. *J*-values versus crack growth for different samples: (a) neat-iPP; (b) iPP/10%Noryl; (c) iPP/10%Noryl/2%SEP; and (d) iPP/10%Noryl/5%SEP.

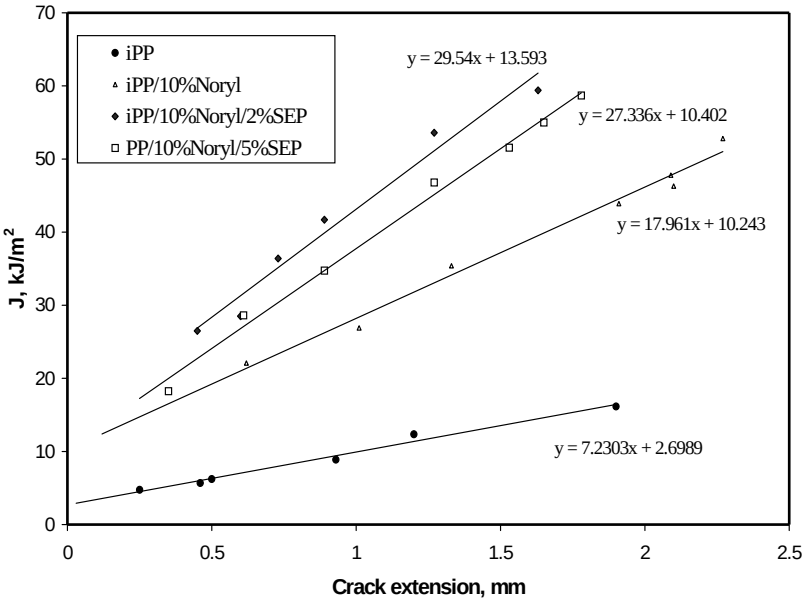

Fig. 8. *J–R* curves of iPP vs. toughened-iPP.

reported in Table 2. As expected, the addition of Noryl increases the modulus of iPP. When 2% SEP by weight of compatibilizer is added into the iPP/10%Noryl blend, Young's modulus is slightly decreased. After 5% by weight of SEP is incorporated, more reduction in Young's modulus is found. It is noted that the yield stresses of all toughened-iPP specimens are reduced by about 15% due to the addition of Noryl and SEP. Several factors may contribute to the reduction of modulus and the yield stress. Generally speaking, for a semi-crystalline polymer, a higher crystallinity gives rise to high modulus and yield stress. The larger the spherulite, the higher the modulus is observed [14]. For polymer blends, no direct correlation between crystallinity and tensile property can be made due to complex morphology and deformation processes. Nevertheless, the effects of crystallinity and spherulite size on modulus and yield stress in polymer blends should show the same trend as those in a single component semi-crystalline polymer.

From the DSC results and optical micrographs (see Table 1 and Fig. 3), all samples show almost the same crystallinity but different spherulite sizes. According to Way's result [14], however, variation in spherulite size below 100 μm has only minor effect on yield stress. Only when the spherulite size is larger than 100 μm will the size effect become significant. In the present study, we observed difference in spherulite sizes among neat- and toughened-iPP. Even though the difference is large, the average spherulite size in all samples is well below 100 μm. Further investigations on spherulite size using the etching technique show that the spherulite features of iPP, iPP/Noryl and iPP/Noryl/SEP blends are different. Fully grown spherulites cannot be observed in the SEP-compatibilized iPP/Noryl blends. However, the yield stress of these blends is almost the same. The modulus of the iPP/Noryl with smaller spherulites is higher than that of the iPP with larger spherulites. On the other hand, the iPP/Noryl/SEP blends with smaller spherulites have lower modulus than that of the iPP. We therefore surmise that the spherulite size effect on modulus and yield stress is at best secondary. The second phase particles are the main cause of the change in modulus. The reduction in yielding stress is mainly ascribed to the presence of second phase particles which act as stress concentrators to decrease the overall yield stress.

3.5. Crack growth resistance curves (J–R curves) and crack initiation energy J_c

Typical load–displacement (*P–d*) curves obtained at room temperature for neat- and toughened-iPP are shown in Fig. 6. The neat-iPP experiences brittle fracture behavior with little sign of plasticity. With an addition of 10% by weight of Noryl, a pronounced non-linear *P–d* curve is observed (Fig. 6). This indicates signs of plastic deformation in iPP/Noryl. After the crack initiates, the crack propagates in a stable manner. As for the iPP/Noryl/SEP blends, the samples show non-linear *P–d* curves with even more stable crack growth. No unstable fracture occurs in these blends. This strongly indicates that the iPP/Noryl/SEP blends exhibit a much higher fracture toughness than iPP and iPP/Noryl. It is of interest to note that large scale plastic deformation takes place before crack growth in iPP/10%Noryl/SEP specimens as indicated by the flat portion of the *P–d* curves (Fig. 6).

The *J–R* curves with blunting line for the iPP blend systems are shown in Fig. 7. It is worth mentioning that the neat-iPP specimen experiences a stable–unstable type of crack growth. After a certain amount of stable crack propagation, crack instability occurs abruptly and the

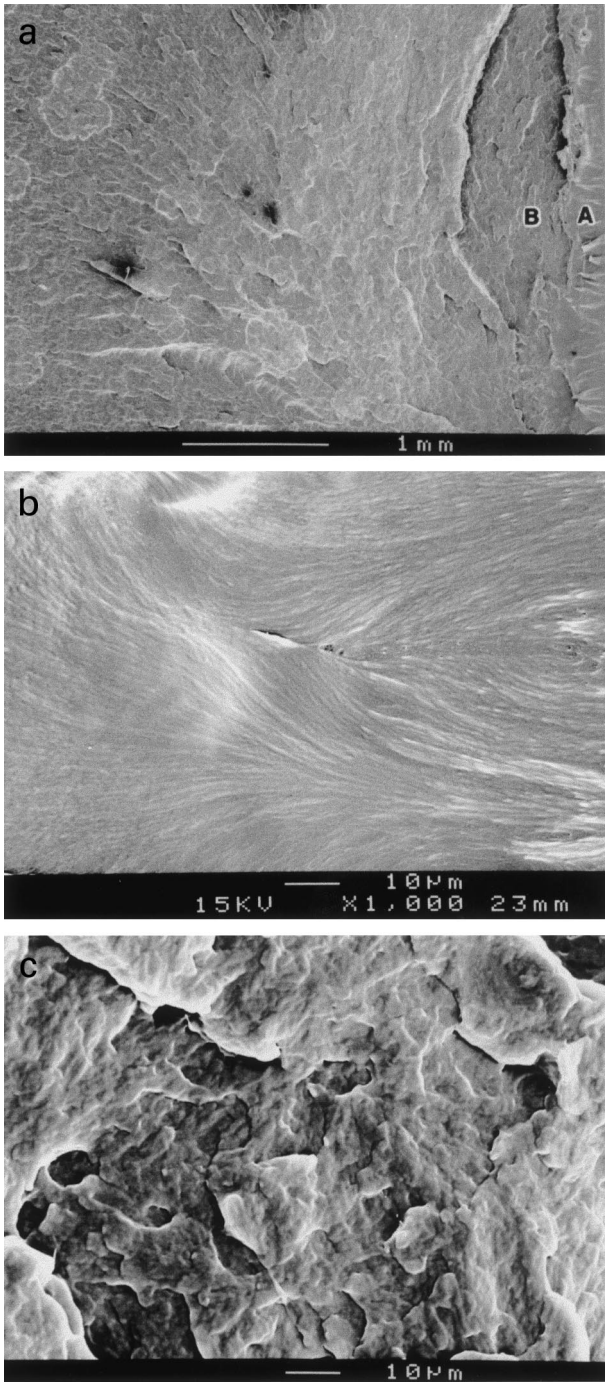

Fig. 9. Scanning electron micrographs of the neat-iPP *J*-test specimen: (a) an overview of the fracture surface; (b) taken at the stable crack growth zone A; and (c) taken at the fast crack zone B.

specimen breaks into two halves. The maximum *J*-value obtained at break for neat-iPP is about 20.3 kJ/m^2. On the other hand, a completely stable fracture is observed in the iPP/10%Noryl and iPP/10%Noryl/SEP blends. Upon loading, the crack tip is seen to blunt extensively with a large amount of crack tip plasticity for SEP-compatibilized iPP/Noryl blends. J_c-values of all specimens calculated from the intersection of *J–R* curves and blunting lines are listed in Table 2. The J_c of iPP is relatively low and consistent with those published in the literature [25–27]. It is evident that the utilization of Noryl and SEP has greatly improved the fracture toughness of iPP. Clearly, Noryl alone is effective in toughening iPP. Addition of the SEP further increased the toughness of the iPP/Noryl blend. For comparison purposes, the *J–R* curves of neat-and toughened-iPP blends are shown in Fig. 8. Obviously, the Noryl-toughened blends have a much higher crack propagation resistance as well as crack initiation resistance than those of neat-iPP. It is noted that the J_c value of the 2% SEP-compatibilized iPP/10%Noryl blend is higher than that of the 5% SEP-compatibilized iPP/10%Noryl blend. This difference is discussed in Part II [28] of this series, which focuses on the toughening mechanism investigations. In this study J_c values, instead of J_{ic} values, are reported due to insufficient specimen thickness for all iPP blends.

3.6. Morphology–structure–property relationship

The improvements in crack initiation and propagation resistance of iPP blends are related to the morphology of blends. It is well known that crystallinity, spherulite size, second phase particle size and interfacial adhesion between the particle and matrix have great influence on both crack initiation and propagation in polymer blends. In the present study, the crystallinity and crystalline size of all specimens are about the same. However, the iPP spherulite features and Noryl particle sizes are dramatically different among the blends analyzed. Varga [29] in his excellent review explained that spherulite boundaries in neat-iPP are the "weak paths", and failure often initiates at these locations by coalescence of microvoids and crazes. The weakness of these interspherulitic zones arises from the non-crystallized components which are accumulated in these regions. Hornbogen and Friedrich [30] and Lustiger et al. [31], independently showed that cracks propagate easily at the interface between coarse spherulites and that fracture resistance can be improved by improving inter-crystalline and interspherulitic links. In the present study, one can see that spherulites are well developed in the neat-iPP specimen (Figs. 3(a) and 4(a)). During fracture, a small amount of plastic deformation occurred near the fracture surface of the stable crack growth region (Fig. 9(b)). The fracture surface ahead of the crack tip plastic zone is smooth (Fig. 9(c)), which is characteristic of brittle failure. No other effective energy dissipation process can be observed. This is consistent with the relatively low J_c and $dJ/d\Delta a$ values of iPP.

When 10% Noryl is added into iPP, the spherulite size is significantly reduced even though the Noryl particles are still large (about 10–15 μm), as shown in Figs. 3(b), 4(b) and 5(b). Scanning electron micrographs of the *J*-integral tested specimen fracture surface reveal the evidence of ductile failure (Fig. 10(b)), where highly drawn fibrils are found on the fracture surface. A careful investigation suggests that the adhesion between iPP and Noryl is quite

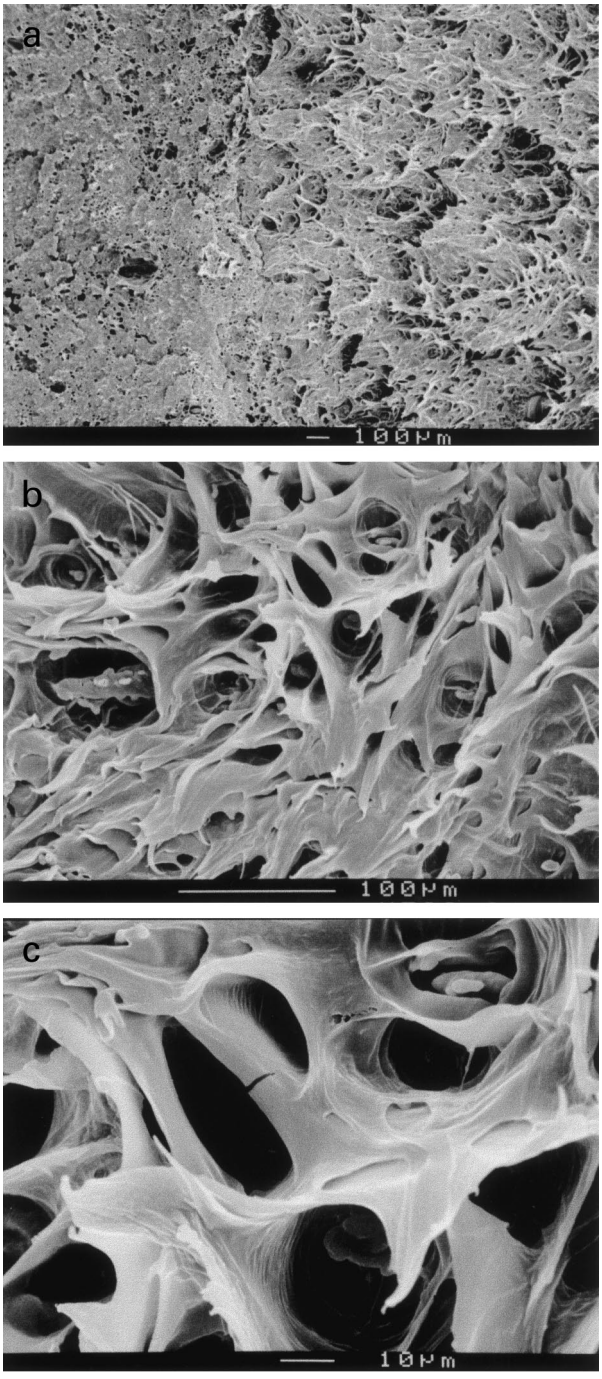

Fig. 10. Scanning electron micrographs of the iPP/10%Noryl *J*-test specimen: (a) an overview of the fracture surface; (b) taken at the stable crack growth zone; and (c) high magnification of (b).

poor (Fig. 10(c)). No signs of Noryl particles are observed on the fracture surface. The poorly adhered Noryl particles must have escaped from iPP matrix during fracture. The SEM photographs in Fig. 10(b) and (c) suggest that Noryl particles induce matrix voiding on the fracture surface.

In the SEP-compatibilized iPP/10%Noryl blends, a ductile failure mode is predominant (Figs. 11 and 12). A

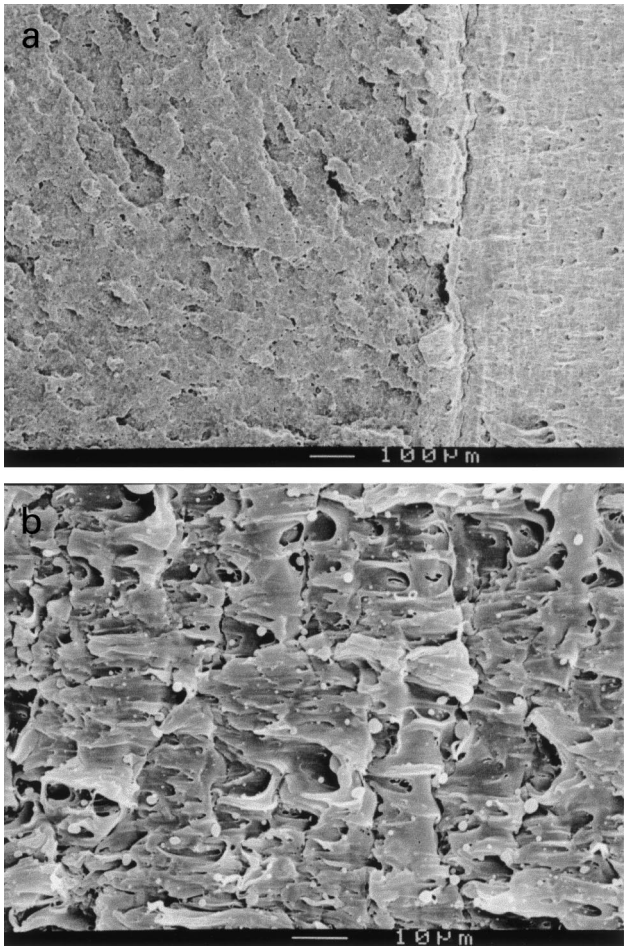

Fig. 11. Scanning electron micrographs of the iPP/10%Noryl/2%SEP *J*-test specimen: (a) an overview of the fracture surface and (b) taken at the stable crack growth zone.

large scale plastic zone ahead of the crack tip is developed (Figs. 11(a) and 12(a)). A careful examination of the fracture surface shows that plastic flow and fibril formation of iPP matrix are present. Interfacial adhesion between Noryl particles and iPP matrix appears to be very good as indicated by the presence of well-bonded Noryl particles found on the fracture surface (Fig. 13). SEP cannot be observed on the fracture surface by SEM due to the lack of contrast. As shown in the TEM micrographs, the SEP phase is located at the interface between Noryl particles and iPP matrix. No significant Noryl particle drawing is observed. This suggests that the strength of SEP is much lower than that of the Noryl particles. As a result, SEP rupture takes place and causes the Noryl particles to be exposed on the fracture surface (Fig. 13). Except for particle sizes, no significant differences on fracture surface between 2 and 5% SEP-compatibilized iPP/10%Noryl blends are observed (Figs. 11(b), 12(b) and 13). The above analyses are all based on fracture surface observations. The detailed fracture mechanisms and deformation sequences are discussed in Part II [28] of this series through sub-critical crack tip damage zone analysis of the iPP blends using OM, SEM and TEM.

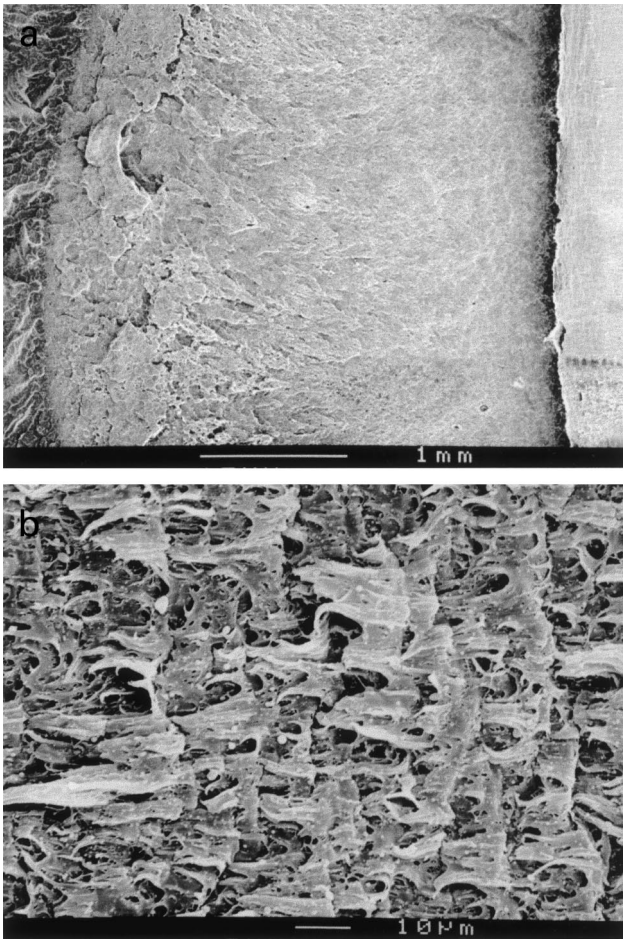

Fig. 12. Scanning electron micrographs of the iPP/10%Noryl/5%SEP *J*-test specimen: (a) an overview of the fracture surface and (b) taken at the stable crack growth zone.

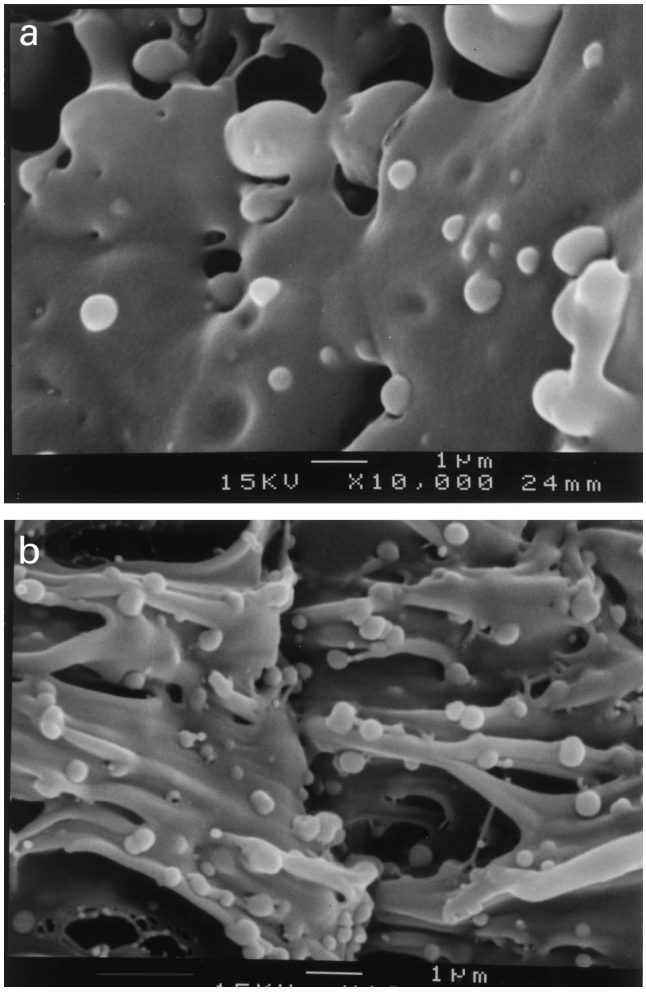

Fig. 13. Scanning electron micrographs of the *J*-test specimen fracture surfaces of (a) iPP/10%Noryl/2%SEP and (b) iPP/10%Noryl/5%SEP. Good interfacial adhesion is evidenced between Noryl particles and iPP matrix.

4. Conclusions

Polypropylene can be toughened through the rigid–rigid polymer toughening concept. Noryl can be utilized to significantly increase iPP toughness without sacrificing stiffness. SEP is an effective compatibilizer for iPP/Noryl blend. The addition of this compatibilizer greatly reduces Noryl particle size and improves particle-matrix interfacial bonding. This further improves the fracture toughness of iPP.

Acknowledgements

The authors would like to thank GE Plastics and Shell Chemical for donating materials for the present work. Special thanks are given to Defense Logistic Agency (Contract SPO 103-96-D-0023) for financial support of this work.

References

[1] Borggreve RJM, Gaymans RJ, Schuijer J, Ingen Housz JF. Polymer 1987;28:1489.
[2] Breuer H, Haaf F, Stabenow J. J Macromol Sci—Phys 1977;B14:387.
[3] Chu J, Rumao R, Coleman B. Scratch and mar resistance of filled polypropylene materials. Report, 1995.
[4] Yee AF, Parker DS, Sue H-J, Huang I.-C. PMSE Div, Preprints, 194th ACS National Meeting, August 1987.
[5] Sue H-J, Yee AF. SPE-RETEC (Chicago), The Society of Plastics Engineers, September 1987.
[6] Sue H-J, Yee AF. J Mater Sci 1989;24:1447.
[7] Sue H-J, Yee AF. J Mater Sci 1991;26:3449.
[8] Sue H-J, Pearson RA, Yee AF. Polym Engng Sci 1991;31:793.
[9] Wu S. Polymer 1985;26:1855.
[10] D'Orazio L, Greco R, Mancarella C, Martuscelli E, Ragosta G, Silvestre C. Polym Engng Sci 1982;22:536.
[11] Bianchi L, Cimmino S, Forte A, Greco R, Martuscelli E, Riva F, Silvester C. J Mater Sci 1985;20:895.
[12] D'Orazio L, Mancarella C, Martuscelli E, Sticotti G. J Mater Sci 1991;26:4033.
[13] Greco R, Ragosta G. J Mater Sci 1988;23:4171.
[14] Way JL, Atkinson JR, Nutting J. J Mater Sci 1974;9:293.
[15] Brandup J. Polymer handbook. New York: Wiley, 1975.
[16] Holik AS, Kambour RP, Hobbs SY, Fink DG. Microstruct Sci 1979;7:357.
[17] Olley RH, Bassett DC. Polymer 1983;23:1707.

[18] Bassett DC, Olley RH. Polymer 1984;25:935.
[19] Greco R, Mancarella C, Martuscelli E. Polymer 1987;28:1929.
[20] Chou CJ, Vijayan K, Kirby D, Hiltner A, Baer E. J Mater Sci 1988;23:2521.
[21] Pukansky B, Belina K, Rockenbauer A, Maurer FHJ. Composites 1994;25:205.
[22] Rybnikar F. J Appl Polym Sci 1982;27:1479.
[23] Wei G-X, Sue H-J. Unpublished work.
[24] Shell Chemical Company. Technical Bulletin.
[25] Ouederni M, Phillips PJ. J Polym Sci: Polym Phys 1995;33:1313.
[26] Ha CS, Kim Y, Cho WJ. J Mater Sci 1996;31:2917.
[27] Hornsby PR, Premphet K. J Mater Sci 1997;32:4767.
[28] Wei G-X, Sue H-J, Chu J, Huang C, Gong K. J Mater Sci 1999; in press.
[29] Varga J. J Mater Sci 1992;27:2557.
[30] Hornbogen E, Friedrich K. J Mater Sci 1980;15:2175.
[31] Lustiger A, Marzinsky CN, Mueller RR. J Polym Sci: Polym Phys 1998;36:2047.